Linear density response function within the time-dependent exact-exchange approximation

Maria Hellgren and Ulf von Barth
Mathematical Physics, Institute of Physics, Lund University, Sölvegatan 14A, S-22362 Lund, Sweden
(Received 22 April 2008; revised manuscript received 1 July 2008; published 9 September 2008)

We have calculated the frequency-dependent exact-exchange (EXX) kernel of time-dependent (TD) density-functional theory employing our recently proposed computational method based on cubic splines. With this kernel we have calculated the linear density response function and obtained static polarizabilites, van der Waals coefficients, and correlation energies for all spherical spin-compensated atoms up to argon. Some discrete excitation energies have also been calculated for Be and Ne. As might be expected, the results of the TDEXX approximation are close to those of TD Hartree-Fock theory. In addition, correlation energies obtained by integrating over the strength of the Coulomb interaction turn out to be highly accurate.

DOI: 10.1103/PhysRevB.78.115107 PACS number(s): 71.15.−m

I. INTRODUCTION

The present paper is one in a series of papers[1–4] reporting on work with the overall aim of finding computationally efficient but still accurate ways of calculating excited-state properties of systems in which excitonic effects play an important role. Traditionally, such effects have been studied by solving approximate versions of the Bethe-Salpeter equation in which the particle-hole interaction is taken to be a statistically screened Coulomb potential.[5] Unfortunately, such *ab initio* methods are computationally very demanding especially in low-symmetry systems such as nanostructures and large molecules. During the last decade, time-dependent density-functional theory[6–8] (TDDFT) has emerged as a competing technique due to its computational efficiency and better scaling with the size of the system. In recent years, the use of TDDFT has virtually "exploded" within theoretical chemistry. On the other hand, within TDDFT, the limitations are rather caused by our rudimentary knowledge of the "mysterious" exchange-correlation (XC) kernel f_{xc}, into which all effects beyond the random phase approximation (RPA) are transferred.

In most applications of TDDFT one resorts to an XC kernel constructed from some ground-state XC potential evaluated at the instantaneous electron density. In this way, the non-locality in time (memory effects) leading to a frequency-dependent XC kernel, is neglected. These are the so-called adiabatic approximations and the simplest example is the adiabatic local-density approximation (ALDA) derived from the ground-state local-density approximation. In fact, any approximate functional within ground-state density-functional theory (DFT) can yield an adiabatic approximation within TDDFT. Although such approximations have been shown to provide good estimates of many physical quantities, there are qualitative features which cannot be accounted for. For the description of, e.g., excitation energies with multiple-particle character, the kernel is expected to have a strong frequency dependence.[9]

Alternative approaches based on many-body perturbation theory (MBPT) to generate new and more advanced kernels have been proposed by some authors.[2,10–13] Up to now, however, the performance of such kernels in describing excited-state as well as ground-state properties has been the subject of little investigation, especially in finite systems.

The simplest approximation derived from MBPT is the time-dependent exact-exchange (TDEXX) approximation. It can be obtained from a stationary action principle by retaining only the exchange part of the XC part of the total action, i.e., terms up to first order in the Coulomb interaction. The exact-exchange (EXX) kernel f_{x} is frequency dependent and therefore fundamentally differs from the adiabatic approximations. Because the EXX kernel can also be derived from our[2] variational approach to the many-body problem, as is done here, it automatically possesses conserving properties which means, e.g., that the resulting linear density response function will obey the f-sum rule. Furthermore, the corresponding EXX potential of ground-state DFT has already been thoroughly studied and shown to share many properties of the exact XC potential such as, e.g., the correct $-1/r$ asymptotic decay and the derivative discontinuity with respect to particle number.

Implementations of the TDEXX approximation have so far been limited to the calculation of the total energy and the plasmon dispersion relation of the electron gas,[3] the optical-absorption spectrum of bulk silicon,[14] and, recently, van der Waals coefficients and polarizabilities for some simple atoms and molecules.[15] The adiabatic TDEXX and the exact TDEXX of a two-electron system (which turns out to be frequency independent) known as the Petersilka–Gossman–Gross (PGG) approximation have also been used in the calculation of atomic and molecular transition frequencies.[16–18] In the nonlinear regime the TDEXX approximation has most recently been applied to the problem of electron dynamics in a quantum well.[19]

In this paper, we calculate the linear density response function using the *fully* frequency-dependent EXX kernel for all spherical spin-compensated atoms up to argon and present results on correlation energies, van der Waals coefficients, static polarizabilities, and a few discrete excitation energies for beryllium and neon. The correlation energies, calculated from the Hellman-Feynman theorem applied to the strength of the Coulomb interaction, turn out to be very accurate, whereas polarizabilities and van der Waals coefficients are similar in quality to the rather poor results of time-dependent Hartree-Fock (TDHF) theory.

The paper is organized as follows. In Sec. II we sketch the derivation of the relevant equations and discuss the TDEXX

approximation in comparison to TDHF. We also give a short description of the computational methods. In Sec. III we present our results and compare them with other approximations and exact results. Some attention is given to the kernel itself and we provide evidence of the f-sum rule being obeyed by studying the large ω behavior of both f_x and the dynamical polarizability.

As mentioned above, the fact that the TDEXX approximation obeys the f-sum rule follows from the possibility to derive it from the variational and conserving approach to MBPT. In the Appendix we show, however, the details on how the defining equations lead to the f-sum rule. This is rather illuminating and demonstrates the necessity for using the correct local exchange potential from the linearized Sham Schlüter (LSS) equation in the evaluation of the f_x kernel in order to have the sum rule fulfilled.

Finally, in Sec. IV, we draw our conclusions and announce a forthcoming publication on spectral properties.

II. THEORY AND COMPUTATIONAL DETAILS

A. General formulation

Within TDDFT the electronic linear density response function χ is given by

$$\chi = \chi_s + \chi_s(v + f_{xc})\chi, \tag{1}$$

where χ_s is the Kohn-Sham (KS) linear density response function, v is the Coulomb interaction and f_{xc} is the XC kernel defined as the functional derivative of the XC potential v_{xc},

$$f_{xc} = \frac{\delta v_{xc}}{\delta n}. \tag{2}$$

It has been shown in previous publications[2,4] that various consistent and, in particular, conserving approximations to v_{xc} and f_{xc} can be obtained from the Klein action functional[20] by choosing physically reasonable approximations to the defining Φ functional.[21] The stationary property of the Klein functional with respect to Green functions generated by local potentials leads directly to the linearized Sham Schlüter[22] equation

$$\int \chi_s(1,2)v_{xc}(2)d2 = \int \Sigma_s(2,3)\Lambda(3,2;1)d2d3, \tag{3}$$

where the self-energy Σ_s is Φ derivable and expressible in only the KS Green function G_s and the Coulomb interaction. The quantity Λ is the functional derivative of G_s with respect to the KS potential V,

$$i\Lambda(3,2;1) = \frac{\delta G_s(3,2)}{\delta V(1)} = G_s(3,1)G_s(1,2).$$

The equation for the corresponding kernel f_{xc} is obtained by varying Eq. (3) with respect to V. The result is

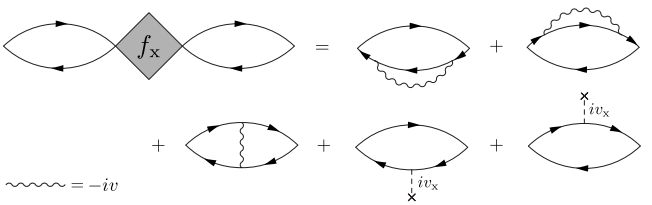

FIG. 1. Diagrammatic representation of Eq. (4) with the self-energy in the Hartree-Fock approximation.

$$\int \chi_s(1,2)f_{xc}(2,3)\chi_s(3,4)d2d3$$
$$= \int \frac{\delta\Sigma_s(2,3)}{\delta V(4)}\Lambda(3,2;1)d2d3$$
$$+ \int \Lambda(1,2;4)\Delta(2,3)G_s(3,1)d2d3$$
$$+ \int G_s(1,2)\Delta(2,3)\Lambda(3,1;4)d2d3, \tag{4}$$

where $\Delta(2,3)=\Sigma_s(2,3)-v_{xc}(2)\delta(2,3)$. Due to the variational property of the Klein functional and the Φ derivability of the self-energy, the kernel f_{xc} obtained from Eq. (4) will result in a response function [Eq. (1)] which is particle conserving. In the linear regime this means, e.g., that it must obey the f-sum rule.

In this work we are interested in studying the so-called TDEXX approximation which is derived at the TDHF level of MBPT. The self-energy is then given by

$$\Sigma_s^x(2,3) = iv(2,3)G_s(2,3), \tag{5}$$

and its variation with respect to V becomes

$$\frac{\delta\Sigma_s^x(2,3)}{\delta V(4)} = -v(2,3)\Lambda(2,3;4). \tag{6}$$

The resulting equation for the EXX kernel f_x is represented diagrammatically in Fig. 1. Notice that the obtained f_x is often referred to as the kernel of the time-dependent optimized effective potential (TDOEP) method. It has been derived several times before by other people starting with Sharp and Horton[23] in the fifties and continuing with Talman and Shadwick[24] in the sixties. The resulting response function has been derived by Rajagopal,[25] Holas *et al.*,[26] Lemmens *et al.*,[27,28] and more recently by Gross[29] to mention a few. Our way of deriving the same approximation has the advantage of demonstrating the conserving properties of the approximation. These properties are also inherent in the original TDHF approximation. Below we will make further comparisons between TDHF and TDEXX, illustrating their similarities and differences.

B. TDEXX as compared to TDHF

The quantity to be determined in the TDHF equation is the three-point function $\chi_2 = \delta G / \delta V_{ext}$, where V_{ext} is the external potential and G is the HF Green function given by the solution of the Dyson equation,

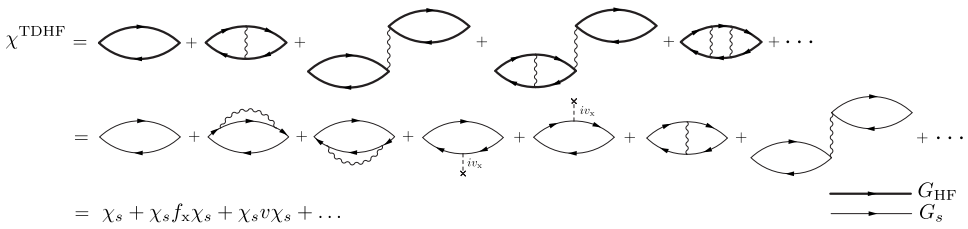

FIG. 2. The linear density response function in TDHF. The first row shows a diagrammatic expansion using the HF Green function. The second row shows an expansion in terms of the KS Green function. All diagrams up to first order are drawn and seen to be the same as the first-order terms of χ in TDEXX.

$$G = G_0 + G_0 \Sigma^{\mathrm{HF}}[G] G, \tag{7}$$

where G_0 is the noninteracting Green function containing just the external (nuclear) potential and $\Sigma^{\mathrm{HF}} = V_{\mathrm{H}} + \Sigma^{\mathrm{x}}$ with V_{H} being the Hartree potential. By varying the Dyson equation with respect to the external potential we arrive at the equation for χ_2, usually referred to as the TDHF equation

$$\chi_2(1,3;2) = G(1,2)G(2,3) + \int d4567 G(1,4)G(5,3)\frac{\delta \Sigma^{\mathrm{HF}}(4,5)}{\delta G(6,7)}\chi_2(6,7;2). \tag{8}$$

The linear density response function can then be obtained as $\chi^{\mathrm{TDHF}}(1,2) = -i\chi_2(1,1;2)$. In Fig. 2, on the first row, χ^{TDHF} is depicted diagrammatically with terms up to second order in the explicit dependence on the Coulomb interaction. There is, of course, also a dependence on v through G, which is summed up to infinite order in the interaction strength through Eq. (7).

Instead of working with G_0 as our zeroth order Green function we can choose to work with the KS Green function G_s. This Green function can also be found through a Dyson-like equation

$$G_s = G_0 + G_0\{V_{\mathrm{H}}[G_s] + v_{\mathrm{x}}[G_s]\}G_s. \tag{9}$$

By inverting Eqs. (7) and (9) we find again the equation for G but with G_s as the zeroth order Green function

$$G = G_s + G_s\{\Sigma^{\mathrm{HF}}[G] - V_{\mathrm{H}}[G_s] - v_{\mathrm{x}}[G_s]\}G. \tag{10}$$

Iterating to first order gives us

$$G^{(1)} = G_s + G_s\{\Sigma^{\mathrm{x}}[G_s] - v_{\mathrm{x}}[G_s]\}G_s. \tag{11}$$

The strictly first-order diagrams (in terms of G_s) for χ^{TDHF} can now be identified (see the second row in Fig. 2) and we see that they are identical to the first-order terms of χ in the TDEXX approximation [see Eq. (1) and Fig. 1]. Thus, we can conclude that, to first order in v, TDHF and TDEXX are the same. Notice that, in principle, this conclusion is independent of the choice of G_s and v_{x} as long as they are related via Eq. (9). But, by using the self-consistent EXX potential the corresponding density is optimized to exactly reproduce the HF density up to first order, thus minimizing the contribution of the approximate higher order terms in χ. However, using any other reasonable v_{x} the corresponding χ in TDEXX is still expected to be rather close to the response function of TDHF. Indeed, as we shall see later (Sec. III F), using the EXX potential, the LDA potential or the exact XC potential leads to very similar response functions. The higher order terms of the TDEXX series can thus be interpreted as an approximation to the corresponding higher order diagrams of TDHF, where the frequency-independent four-point kernel of Eq. (8), i.e., $\delta\Sigma^{\mathrm{x}}/\delta G$, is simulated by the frequency-dependent two-point kernel f_{x}. The trick to approximate the beyond first-order terms in the series of the TDHF response in terms of the zeroth and first order terms such that the whole series can be summed as a geometric one has been suggested before.[26] The full TDHF series can be written order by order as

$$\chi^{\mathrm{TDHF}} = \chi_0[1 + \chi_0^{-1}\chi_1 + \chi_0^{-1}\chi_2 + \cdots] \approx \frac{\chi_0}{1 - \chi_0^{-1}\chi_1} = \chi_0 + \chi_1 + \chi_1\chi_0^{-1}\chi_1 + \cdots.$$

If $\chi_0 = \chi_s$ this is just the TDEXX series.

As shown in the Appendix it is essential to derive the potential v_{x} from the LSS in order to have the f-sum rule obeyed. Self-consistency is, however, not necessary. Choosing any density there is a local one-body potential which, in a noninteracting system, generates that density as well as one-electron orbitals with corresponding eigenvalues. The LSS within EXX [Eq. (3)] then gives a potential v_{x} which, together with these orbitals and eigenvalues, yields an f_{x} from Eq. (4). In this way, both v_{x} and f_{x} are well defined functionals of the starting density. If the density is given by the EXX we have self-consistency, and the resulting f_{x} is the one presented here. If we instead start with a better density, much closer to the exact one, the corresponding eigenvalue differences will be much closer to real particle-hole excitation energies[4] and we will obtain an f_{x} which will still obey the f-sum rule while giving rise to an optical spectrum with a continuum starting in almost the correct place because the highest occupied exact DF eigenvalue equals the negative of the ionization potential.[30] This topic is further discussed together with numerical results in Sec. III F.

C. Numerical method

The numerical implementation of the TDEXX approximation starts with a calculation of the self-consistent ground-state potential v_{x} from Eq. (3). This potential determines the KS system from which G_s and χ_s are calculated and inserted into Eq. (4). The kernel is then obtained through multiplica-

tion by the inverse of χ_s both from the left and the right. Finally, to obtain the full response function χ a RPA-like equation needs to be solved, Eq. (1). Since f_x is frequency dependent all steps after the calculation of the potential need to be repeated at every frequency. Notice also that, due to the spherical symmetry of our studied systems, Eq. (1) separates into several decoupled equations, one for each angular-momentum channel.

We have chosen a basis set implementation using cubic splines as radial basis functions. This basis set has shown to be ideally suited for solving the LSS equation,[4] an equation known to be numerically unstable when using other methods and basis functions.[31–35] We have here found that cubic splines also provide an efficient method for solving the equation for f_x. In retrospect this might not be surprising since this equation has similarities to the LSS equation.

A detailed description of the construction of our basis set can be found in Ref. 4 and a general discussion of B splines in electronic structure calculations can be found in Refs. 36 and 37. Here, we will only list the advantages of using these basis functions. 1) To start with, they are local functions. This gives us a great amount of flexibility in choosing the distribution of splines. Where high accuracy is needed, like in our case close to the nucleus, the density of splines can be chosen arbitrarily high without loosing accuracy in other regions. 2) Another important property of the splines is that there is no risk of instabilities due to overcompleteness because of the strong localization of the splines. 3) Since every spline only overlaps with its three nearest neighbors all matrices will be band diagonal, reducing the amount of storage needed and allowing for the use of efficient diagonalization algorithms. 4) Once a mesh distribution (e.g., a power law or an exponential distribution) and a maximum radius are set there is only one numerical parameter to vary, i.e., the number N of cubic splines. 5) The basis set is complete. The results should thus converge to the exact results as $N\rightarrow\infty$. 6) We have shown that the product of two orbitals can be reexpanded in the same basis set without increasing the number of basis functions. All two-particle functions, like for instance response functions, thus become matrices of the same order as one-particle propagators. 7) A cubic spline is composed of cubic polynomials and hence all integrals can be solved exactly, either analytically or, and actually faster by, using simple Gaussian quadrature.

The work to calculate the density response function within just the RPA (without exchange) is just about as extensive as that required to obtain the response function from any so-called adiabatic or frequency-independent approximation. The calculation of the exchange kernel f_x of the EXX involves sums over two continua for every frequency. An ordinary RPA calculation using N basis functions requires for every frequency const$\times N^3$ operations because of the necessity to invert an $N\times N$ matrix. Including also an exchange-correlation kernel requires for each frequency a double sum over the continuum, i.e., const$\times N^2$ operations plus two additional matrix inversions. This increases the prefactor of the N^3 dependence on the number N of included splines. The prefactor also depends heavily on the number of occupied states but, for large N, including the exchange kernel does not constitute a qualitative difference compared to an ordinary RPA calculation as far as the calculational effort is concerned.

To get an accurate description of both the occupied and the first few unoccupied orbitals we used a cubic distribution of mesh points in all our calculations. The results were converged with ~40 splines for He and with ~60 splines for Ar.

TABLE I. Static polarizabilities for some different atoms calculated in TDEXX, TDHF, RPA, and from the KS system. (a.u.)

Atom	KS	RPA	TDEXX	TDHF	Litt.[c]
He	1.487	1.199	1.322	1.322[a]	1.38
Ne	2.838	2.234	2.372	2.377[a]	2.67
Ar	16.965	9.883	10.737	10.758[a]	11.08
Be	81.385	33.489	45.648	45.62[b]	37.8
Mg	140.26	60.262	81.658	81.60[b]	71.53

[a]From Ref. 38.
[b]From Ref. 39.
[c]From Ref. 40.

III. RESULTS

In this section we present our results on static polarizabilities, van der Waals coefficients and correlation energies for all spin-compensated spherical atoms up to Ar and some discrete excitation energies for Be and Ne. If not indicated all results are obtained with the self-consistent EXX Green function. The convergence criterion for the EXX potential was set to $|n^{(k)}(\boldsymbol{r})-n^{(k-1)}(\boldsymbol{r})|\leq 10^{-7}$.

A. Static polarizabilities

The static polarizability is defined according to

$$\alpha(0)=-\int z\chi(\boldsymbol{r},\boldsymbol{r}',\omega=0)z'd\boldsymbol{r}d\boldsymbol{r}'. \tag{12}$$

For a system with spherical symmetry only the angular-momentum channel $L=1$ of χ contributes. The small polarizabilities of the noble gas atoms as compared to the alkali earth atoms are due to the large gap in the excitation spectrum. On the contrary, Be and Mg have a near degeneracy in the HOMO-LUMO gap causing very large polarizabilities.

In Table I we compare $\alpha(0)$ calculated in TDEXX with $\alpha(0)$ calculated in RPA, TDHF, and from the KS response function, χ_s. Calculating the static polarizability from the KS response function provides a reasonable estimate, albeit too large compared to the true static polarizability of noble gas atoms. In Be and Mg the error is much larger and leads to an overestimation by a factor of 2. Including interaction effects at the level of RPA reduces the KS results for all atoms. However, the RPA polarizabilities are consistently too low as compared to more accurate values. Introducing exchange effects at the level of TDEXX increases $\alpha(0)$ again leading to an appreciable improvement for the noble gas atoms but the error for Be and Mg remains roughly the same but with a different sign.

TABLE II. van der Waals coefficients calculated in different approximations. (a.u.)

Atom	KS	RPA	TDEXX	TDHF	Litt.
He	1.664	1.171	1.375	1.375	1.458[c]
Ne	7.492	5.003	5.506	5.524[a]	6.383[c]
Ar	128	54.23	61.88	61.88[a]	64.30[c]
Be	660	179	283	284[b]	214[d]
Mg	1723	482	765	758[e]	627[d]

[a]From Ref. 15.
[b]From Ref. 41.
[c]From Ref. 42.
[d]From Ref. 43.
[e]From Ref. 44.

TABLE III. Correlation energies calculated within different approximations and compared to accurate CI calculations. The correlation energy is here defined as the total energy minus the HF energy. In the last column also the Hartree-Fock total energies are tabulated. (a.u.)

Atom	TDEXX	RPA	MP2[a]	CI[b]	HF[b]
He	0.044	0.083	0.047	0.0420	2.8617
Ne	0.389	0.596	0.480	0.3905	128.5471
Ar	0.721	1.091	0.844	0.7225	526.8175
Be	0.102	0.181	0.124	0.0943	14.5730
Mg	0.445	0.681	0.514	0.4383	199.6146

[a]From Ref. 31.
[b]From Ref. 45.

The TDEXX polarizabilities are seen to be very close to those of TDHF. This is not surprising as TDDFT within the EXX can be considered as a variational solution to the integral equation of TDHF theory. For a two-electron system such as He, TDEXX is actually identical to TDHF.

B. van der Waals coefficients

The van der Waals coefficient, or C_6 coefficient, between ions A and B is given by the formula

$$C_6 = \frac{3}{\pi}\int_0^\infty \alpha_A(i\omega)\alpha_B(i\omega)d\omega, \tag{13}$$

where $\alpha_A(i\omega)$ is the dynamic polarizability of ion A calculated at imaginary frequencies. In Table II the C_6 coefficients in the TDEXX approximation are presented and compared to the values of the KS system, values calculated in the RPA and the TDHF approximation, as well as accurate values found in the literature. Although TDEXX significantly improve over the RPA for He, Ne, and Ar the C_6 coefficients remain too small. The results for Mg and Be in TDEXX are too large and give no improvement over RPA in an absolute sense. The TDEXX values are again seen to be in good agreement with the full TDHF results. This was also noted in Ref. 15 for He, Ne, and Ar.

C. Correlation energies

Using the standard trick based on the Hellman-Feynman theorem to integrate the interaction energy with respect to the strength of the Coulomb interaction the correlation energy becomes

$$E_c = -\int_0^1 d\lambda \int_0^\infty \frac{d\omega}{2\pi}\mathrm{Tr}\{v[\chi^\lambda(i\omega) - \chi_s(i\omega)]\}. \tag{14}$$

In Eq. (14) we have used the short hand notation $\mathrm{Tr}fg = \int d\mathbf{r}d\mathbf{r}' f(\mathbf{r},\mathbf{r}')g(\mathbf{r}',\mathbf{r})$ for any two-point functions f and g and defined the response function

$$\chi^\lambda = \frac{\chi_s}{1-(\lambda v + f_{\mathrm{xc}}^\lambda)\chi_s},$$

where f_{xc}^λ is the XC kernel of a system of electrons interacting through the rescaled Coulomb potential λv. From this expression the simplest approximation is obtained by setting $f_{\mathrm{xc}}=0$, leading to the formula for the RPA correlation energy. A fully self-consistent calculation of this approximation was performed in Ref. 4 for all spin-compensated spherical atoms up to Ar. With $f_{\mathrm{xc}}=f_{\mathrm{x}}$ a cancellation between Hartree and exchange terms is expected to occur, improving the largely overestimated RPA values. We have here, for the first time, performed such a calculation. The results are presented in Table III and compared with those in the RPA and the MP2 approximation[31] as well as results from accurate configuration-interaction (CI) calculations.[45] As expected, the TDEXX results are very accurate. A diagrammatic analysis (see Fig. 3) shows that with this kernel the correlation energy will, apart from the RPA or bubble series of diagrams, also contain the important second-order exchange diagram (included in the MP2 approximation) as well as an infinite series of terms simulating the higher order exchange diagrams.

D. *f*-sum rule and EXX kernel

In the Appendix we prove that the f-sum rule, a consequence of particle conservation, is valid in the TDEXX approximation by showing that the coefficient of the $1/\omega^2$ term in the large ω expansion of χ is the same as in the expansion of χ_s. Thus, by expressing the dynamical polarizability, Eq. (12), as

$$\alpha(i\omega) = \sum_q \frac{f_q}{\omega^2+\omega_q^2}, \tag{15}$$

where $q=(k,\mu)$ is a particle-hole index, ω_q is an excitation energy, and f_q is the corresponding oscillator strength, the sum over all oscillator strengths must equal the number of particles

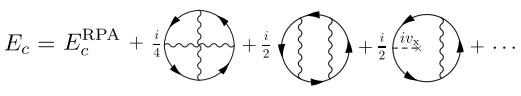

FIG. 3. Diagrams contained in the correlation energy functional, Eq. (14), with $f_{\mathrm{xc}}=f_{\mathrm{x}}$.

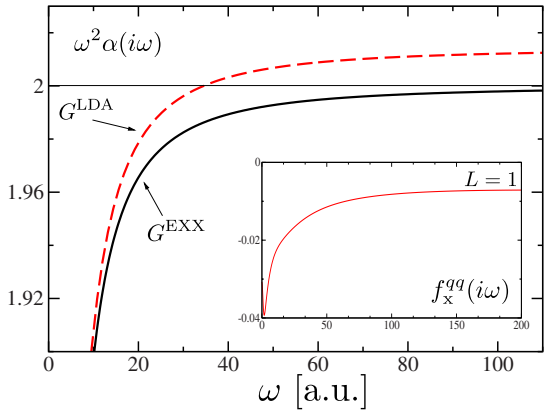

FIG. 4. (Color online) The main figure shows $\omega^2\alpha(i\omega)$ for He calculated at different Green functions. The inset shows f_{x}^{qq} with $L=1$ and $q=2s\rightarrow 2p$ for Be. The large ω behavior in both plots clearly indicates that the f-sum rule is obeyed in our calculations.

$$\sum_q f_q = N.$$

As a test of our numerical accuracy this result was checked. We multiplied $\alpha(i\omega)$ by ω^2 and studied the large ω values of this function. Indeed, within high accuracy ($\leq 10^{-4}$), the results converged to N for all atoms.

In Fig. 4 we have plotted $\omega^2\alpha(i\omega)$ for He. The kernel f_{x} was calculated using either the Green function G_s and the exchange potential v_{x} of the EXX or the same quantities within LDA. The f-sum rule is not expected to be obeyed in the latter case. And this is, indeed, what is observed. It should be noticed, however, that the violation is minor ($\sim 0.8\%$).

The quantity $\chi_s f_{\mathrm{x}} \chi_s$ must decay as $1/\omega^4$ (see the Appendix). As a consequence, f_{x} cannot diverge (as it does, e.g., in a model system, see Ref. 46) and must approach a constant as $\omega\rightarrow\infty$. Another way to check the f-sum rule and to test our calculations is thus to study the large ω behavior of f_{x}. To do this we first notice that the kernel only enters in the form of matrix elements of the F_q functions:

$$f_{\mathrm{x}}^{qq'}(\omega) = \int F_q(\boldsymbol{r}) f_{\mathrm{xc}}(\boldsymbol{r},\boldsymbol{r}',\omega) F_{q'}(\boldsymbol{r}') d\boldsymbol{r} d\boldsymbol{r}',$$

where F_q is a KS excitation function, i.e., a product of the occupied KS orbital φ_k and the unoccupied KS orbital φ_μ. Now, since the excitation functions alone integrates to zero the kernel is unique only up to the addition of two arbitrary functions, $g_1(\omega,\boldsymbol{r})$ and $g_2(\omega,\boldsymbol{r}')$. The quantity $f_{\mathrm{x}}^{qq'}$ is unique though and in Fig. 5 we have plotted this quantity for Be at imaginary frequencies and different L. The frequency dependence is very weak at low frequencies but becomes more pronounced for higher frequencies. This justifies the use of the adiabatic approximation for low energies. At large ω every matrix elements $f_{\mathrm{x}}^{qq'}(i\omega)$ is seen to approach a constant. This is again demonstrated for one matrix element in the inset of Fig. 4.

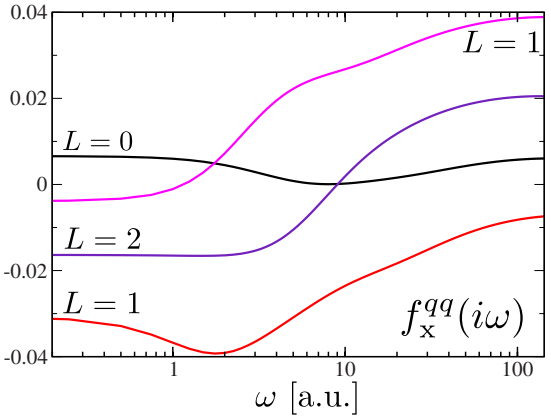

FIG. 5. (Color online) The quantity f_{x}^{qq} for Be is plotted for different L at imaginary frequencies. There are two curves with $L=1$. In the lower, q corresponds to the $2s\rightarrow 2p$ transition and in the upper to the $1s\rightarrow 2p$ transition.

E. Excitation energies

The poles of the exact linear density response function correspond to the particle conserving excitation energies of the system. Thus, any approximate χ yields an approximate set of excitation energies. χ_s contains the excitation energies of the KS system and in many cases they give a good approximation to the discrete part of the spectrum. Nevertheless, χ_s is a noninteracting response function and as such lacks many features of the full many body χ.

With an adiabatic kernel, Eq. (1) can be rewritten as an eigenvalue problem where the eigenvalues correspond to the poles of χ.[47] Due to the frequency dependence of the XC kernel of the EXX this technique to obtain the excitation energies cannot be applied in a straight-forward way. In the present work we have chosen to work with localized basis functions which causes Im χ as a function of frequency to consist of a series of sharp delta functions. And this behavior is independent of whether the frequency lies in the continuum or in the discrete part of the spectrum. In order to obtain something which can be plotted we arbitrarily add a small positive imaginary part to the real frequency and obtain the discrete excitation energies from the positions of the resulting huge peaks in Im χ.

In Table IV we present the first few discrete excitation energies of Be and Ne and compare them to experimental values and to the ones obtained in RPA, TDHF, and the KS system (here, meaning the differences between the KS one-electron eigenvalues). In the case of Be the KS values are too low. The RPA improves over the KS results but proceeding to the TDEXX makes them, somewhat worse. It is interesting to observe how close the results of the TDEXX are to those of the TDHF. In the case of Ne we have observed a qualitatively different behavior. The KS eigenvalue differences are larger than the experimental values. As in the case of Be, the RPA tends to increase the excitation energies yielding, for Ne, an even larger discrepancy. The inclusion of exchange effects does not lower the RPA results, as in the Be case, but rather increase them. Although TDEXX and TDHF push the RPA excitation energies in the same direction the actual values are not as close as for Be.

TABLE IV. The first few discrete excitation energies for Be and Ne in TDEXX compared to experimental, TDHF, RPA, and KS transitions.

	Transition	KS	RPA	TDEXX	TDHF[a]	Exp.[b]
Be						
	$2s \rightarrow 2p$	0.1312	0.2032	0.1764	0.1764	0.1940
	$2s \rightarrow 3p$	0.2412	0.2547	0.2470	0.2471	0.2742
	$2s \rightarrow 4p$	0.2731	0.2777	0.2749	0.2750	0.3063
	$2s \rightarrow 5p$	0.2868	0.2889	0.2877	0.2878	0.3195
Ne						
	$2p \rightarrow 3s$	0.6585	0.6675	0.6803	0.6739	0.6190
	$2p \rightarrow 4s$	0.7793	0.7812	0.7827	0.7818	0.7268
	$2p \rightarrow 5s$	0.8134	0.8141	0.8147	0.8139	0.7593

[a]From Refs. 41 and 49
[b]Adopted from Refs. 41 and 49.

The oscillator strengths for the discrete excitation energies can be extracted from the height of the peaks in the optical spectrum. As an example, we obtain 1.379 for the lowest transition of Be. This can be compared to the TDHF value of 1.378.[41]

F. Sensitivity to the ground-state KS approximation

As noticed by others,[17] it is crucial to have good KS transitions as a starting point when calculating the discrete excitation energies. With the exact KS potential[48] for Ne the $2p \rightarrow 3s$ transition in the KS system becomes 0.612, an already very good approximation to the true value (0.619). The transition frequencies we have obtained are thus expected to be improved by using a ground-state potential better than that of EXX. When we improve the ground-state density and the corresponding orbitals and eigenvalues we still calculate v_x from the LSS in order not to violate the sum rule as discussed in Sec. II B.

We have used the exact densities of Umrigar *et al.*[48] and found the static polarizabilities 1.35 and 40.5 for He and Be, respectively. There is, thus, a significant improvement, particularly in the case of Be. This shows that the largest error is actually caused by a poor description of the ground state within the EXX. With the very accurate densities by Umrigar *et al.* the transition $2s \rightarrow 2p$ in Be becomes 0.182 and the $2p \rightarrow 3s$ transition in Ne becomes 0.631. The transition frequencies are thus also largely improved by using an accurate KS ground state.

By also using the accurate XC potentials by Umrigar *et al.* in Eq. (4) for generating f_x we violate the f-sum rule but, in this way, as discussed in Sec. II B, we obtain a response function which to first order in the Coulomb interaction is identical to that of TDHF. We, therefore, expect the results to revert to our original results from TDEXX which are close to those of TDHF. Indeed, we now obtain the static polarizabilities 1.323 and 45.76 for He and Be, compared to our previous results 1.322 and 45.65, respectively. Using instead the LDA potential for generating f_x we obtain 1.343 and 45.23 for the same quantities, again demonstrating the closeness to the TDHF.

IV. CONCLUSIONS AND OUTLOOK

In this paper we have calculated the linear density response function of the TDEXX approximation for all spin-compensated spherical atoms up to Ar. For the properties studied in this work, i.e., static polarizabilities, van der Waals coefficients and the low-lying excitation energies, the results show that TDEXX is a good approximation to TDHF.

TDEXX only takes into account exchange effects in the response of the system to external perturbations. For noble gas atoms the static polarizabilities and van der Waals coefficients still turn out to be in rather good agreement with the experimental values. The relative error is about 5% for He, 13% for Ne, and 3% for Ar. On the other hand for alkali earth atoms the results are not as satisfactory, the relative error being around 26% for Be and 18% for Mg. For these systems it is thus necessary to include correlation effects in order to get an accurate description of the above properties. The low-lying excitation energies are accurate to within 10% for both Be and Ne. We show here, however, that significantly better excitation energies as well as static polarizabilities can be obtained by using a more accurate exchange-correlation potential for the ground state.

We have also calculated the total energies from the Hellman Feynman theorem applied to the strength of the Coulomb interaction. The results are in excellent agreement with accurate CI calculations. This is probably due to the fact that the fluctuation-dissipation formula at the level of TDEXX accounts for several correlation diagrams as, for instance, the important second-order exchange diagram.

Finally, we have examined the behavior of kernel f_x along the imaginary frequency axis and found it to be both weakly and slowly dependent on ω. It is, however, not without structure indicating a more complex behavior on the real axis as compared to that resulting from simple poles. Indeed, we have seen that the kernel has both single and double poles on the real axis. The weak frequency dependence at the imaginary axis suggests that the adiabatic, i.e., frequency-independent approximations to the EXX approximation, might not be such a bad idea at least not as far as total energies are concerned. The experience from the electron gas, however, strongly contradicts this conjecture.[50]

In most cases of approximations within DFT and TDDFT it is very difficult to see through what kind of physical processes are actually incorporated into that particular approximation. In our case, basing our approximations on Φ-derivable theories within MBPT, we can say with confidence that a description of double excitations is way above the EXX. Such a description would require an f_{xc} based at least on the time-dependent GW approximation[51] which, by the way, probably would yield much better van der Waals coefficients. But again we refer this discussion to a future publication.

ACKNOWLEDGMENTS

This work was started in collaboration with S. Kurth when he was still in Lund and we thank S. Kurth for sharing his experience from this problem. We also thank C.-O. Almbladh for useful discussions. This work was supported by the

European Community Sixth Framework Network of Excellence NANOQUANTA (Grant No. NMP4-CT-2004-500198).

APPENDIX: *f*-SUM RULE

In Ref. 2 we demonstrated that every f_{xc} of TDDFT obtained from the variational formulation of that work obeys particle conservation, which amounts to the f-sum rule in the linear limit.

In this Appendix we will demonstrate how the f-sum rule explicitly comes out of the construction of the kernel f_x of the EXX approximation within TDDFT. Among other virtues, this detailed derivation demonstrates the crucial importance of using the LSS equation when constructing the kernel f_x in order to have the sum rule fulfilled. From Eq. (1) we see that the total density response function χ can be written as

$$\chi = [1 - (v + f_x)\chi_s]^{-1}\chi_s.$$

Since the ground-state KS theory gives the correct density it follows that χ_s obeys the f-sum rule. Given the Lehmann representations for the response functions χ and χ_s this ensures that the coefficient of the $1/\omega^2$ term of the large ω expansion of χ_s has the correct value. If the full response function χ is also to obey the f-sum rule there must, obviously, be no contribution to the $1/\omega^2$ coefficient from the denominator which thus must tend to unity at large ω. A sufficient condition for this is that $f_x\chi_s$ vanishes as $1/\omega^2$ in this limit. From Fig. 1 we see that the quantity which is actually calculated from the diagrams is $\chi_s f_x \chi_s$ which thus should decay as $1/\omega^4$ given the $1/\omega^2$ of dependence of χ_s in this limit. In order to see that this is indeed the case we explicitly examine the large frequency behavior of the different contributions to $\chi_s f_x \chi_s$. As seen from Fig. 1 this quantity has contributions from five Feynman diagrams of which those proportional to the exchange potential v_x are most easily combined with one each of the two self-energy diagrams. The contribution from one of the diagrams with self-energy insertions is

$$S_1(\boldsymbol{r},\boldsymbol{r}';\omega) = 2i\int \frac{d\omega'}{2\pi} G_s(\boldsymbol{r}_1,\boldsymbol{r};\omega')G_s(\boldsymbol{r}',\boldsymbol{r}_2;\omega') \times G_s(\boldsymbol{r},\boldsymbol{r}';\omega+\omega')\Delta(\boldsymbol{r}_1,\boldsymbol{r}_2),$$

where $\Delta = v(\boldsymbol{r},\boldsymbol{r}')\Sigma_k n_k\varphi_k(\boldsymbol{r})\varphi_k^*(\boldsymbol{r}') + v_x(\boldsymbol{r})\delta(\boldsymbol{r}-\boldsymbol{r}')$ and n_k is 1 for occupied states and zero otherwise. Due to time-reversal symmetry the noninteracting Green functions are symmetric in there spatial arguments. It is then easily seen that the contributions from the remaining two diagrams with self-energy insertions are obtained by adding to $S_1(\omega)$ above the result $S_1(-\omega)$. Consequently, the sum of all diagrams with self-energy insertions is an even function of ω. Carrying out the frequency integrations we obtain

$$S_1(\boldsymbol{r},\boldsymbol{r}';z) = \sum_{k_1k_2k_3}\langle k_2|\Delta|k_3\rangle\varphi_{k_1}(\boldsymbol{r})\varphi_{k_1}^*(\boldsymbol{r}')\varphi_{k_2}(\boldsymbol{r})\varphi_{k_3}^*(\boldsymbol{r}') \times \frac{2}{\varepsilon_{k_3}-\varepsilon_{k_2}}\left\{\frac{n_{k_1}-n_{k_3}}{z+\varepsilon_{k_1}-\varepsilon_{k_3}} - \frac{n_{k_1}-n_{k_2}}{z+\varepsilon_{k_1}-\varepsilon_{k_2}}\right\}.$$

Here, the functions $\varphi_k(\boldsymbol{r})$ are the KS orbitals with eigenvalue ε_k and we have switched from time-ordered quantities to retarded ones by everywhere replacing $\omega - i\delta$ by $\omega + i\delta$. The quantity z is a complex frequency in the upper half plane.

When $z \to \infty$ the contribution appears to behave as $1/z$ but we remind the reader that we should add a similar expression with z replaced by $-z$. Then, the leading order becomes A/z^2 with the coefficient

$$A = 4\sum_{k_1k_2k_3}\langle k_2|\Delta|k_3\rangle\varphi_{k_1}(\boldsymbol{r})\varphi_{k_1}^*(\boldsymbol{r}')\varphi_{k_2}(\boldsymbol{r})\varphi_{k_3}^*(\boldsymbol{r}') \times \left\{\frac{(n_{k_1}-n_{k_3})(\varepsilon_{k_3}-\varepsilon_{k_1})}{\varepsilon_{k_3}-\varepsilon_{k_2}} - \frac{(n_{k_1}-n_{k_2})(\varepsilon_{k_2}-\varepsilon_{k_1})}{\varepsilon_{k_3}-\varepsilon_{k_2}}\right\},$$

where we have multiplied by 2 to account for the remaining two self-energy-like diagrams $[S_1(-\omega)]$. We can regroup the terms and write $A = A_1 + A_2$ where

$$A_1 = 4\sum_{k_1k_2k_3}\langle k_2|\Delta|k_3\rangle\varphi_{k_1}(\boldsymbol{r})\varphi_{k_1}^*(\boldsymbol{r}')\varphi_{k_2}(\boldsymbol{r})\varphi_{k_3}^*(\boldsymbol{r}') \times (n_{k_1}-n_{k_3})$$

$$A_2 = 4\sum_{k_1k_2k_3}\langle k_2|\Delta|k_3\rangle\varphi_{k_1}(\boldsymbol{r})\varphi_{k_1}^*(\boldsymbol{r}')\varphi_{k_2}(\boldsymbol{r})\varphi_{k_3}^*(\boldsymbol{r}') \times (n_{k_3}-n_{k_2})\frac{\varepsilon_{k_1}-\varepsilon_{k_2}}{\varepsilon_{k_3}-\varepsilon_{k_2}}.$$

Let us now define the one-particle density matrix by

$$n(\boldsymbol{r},\boldsymbol{r}') = 2\sum_k n_k\varphi_k(\boldsymbol{r})\varphi_k^*(\boldsymbol{r}')$$

and use the completeness of the KS orbitals. We obtain

$$A_1 = \delta(\boldsymbol{r}-\boldsymbol{r}')\int d^3\boldsymbol{r}_3 v(\boldsymbol{r}-\boldsymbol{r}_3)|n(\boldsymbol{r}_3,\boldsymbol{r})|^2 - v(\boldsymbol{r}-\boldsymbol{r}')|n(\boldsymbol{r},\boldsymbol{r}')|^2 \tag{A1}$$

and see that the diagrams containing v_x do not contribute to leading order in the large frequency limit.

In order to manipulate the A_2 coefficient we use the fact that the KS orbitals obey the KS equation

$$\left\{-\frac{1}{2}\nabla^2 + V(\boldsymbol{r})\right\}\varphi_k(\boldsymbol{r}) = \varepsilon_k\varphi_k(\boldsymbol{r}),$$

where $V(\boldsymbol{r})$ is the full KS potential. Because of the difference $\varepsilon_{k_1}-\varepsilon_{k_2}$, the terms involving the potential will vanish and we obtain

$$A_2 = 2\sum_{k_1k_2k_3}\langle k_2|\Delta|k_3\rangle\varphi_{k_1}^*(\boldsymbol{r}')\varphi_{k_3}^*(\boldsymbol{r}')\frac{n_{k_3}-n_{k_2}}{\varepsilon_{k_3}-\varepsilon_{k_2}} \times [\varphi_{k_1}(\boldsymbol{r})\nabla^2\varphi_{k_2}(\boldsymbol{r}) - \varphi_{k_2}(\boldsymbol{r})\nabla^2\varphi_{k_1}(\boldsymbol{r})].$$

Now, using

$$\varphi_1\nabla^2\varphi_2 - \varphi_2\nabla^2\varphi_1 = 2\,\nabla\,(\varphi_1\,\nabla\,\varphi_2) - \nabla^2(\varphi_1\varphi_2)$$

and the completeness we can write A_2 as

$$A_2 = 2\nabla[\delta(\mathbf{r}-\mathbf{r}')\nabla f(\mathbf{r})] - 2\nabla^2[\delta(\mathbf{r}-\mathbf{r}')f(\mathbf{r})],$$

where

$$f(\mathbf{r}) = \sum_{k_2k_3} \langle k_2|\Delta|k_3\rangle \varphi_{k_2}(\mathbf{r})\varphi^*_{k_3}(\mathbf{r})\frac{n_{k_3}-n_{k_2}}{\varepsilon_{k_3}-\varepsilon_{k_2}}.$$

This is because, by symmetry,

$$\nabla f(\mathbf{r}) = 2\sum_{k_2k_3} \langle k_2|\Delta|k_3\rangle \varphi^*_{k_3}(\mathbf{r})\nabla\varphi_{k_2}(\mathbf{r})\frac{n_{k_3}-n_{k_2}}{\varepsilon_{k_3}-\varepsilon_{k_2}}.$$

But, $f(\mathbf{r})=0$ is the LSS equation defining v_x and we have shown that $A_2=0$.

Let us now study the remaining fifth diagram—the vertex diagram—in the high-frequency limit. The contribution R_V from this diagram is

$$R_V(\mathbf{r},\mathbf{r}';\omega) = 2\int d^3\mathbf{r}_1 d^3\mathbf{r}_2 \int \frac{d\omega_1}{2\pi}\int\frac{d\omega_2}{2\pi} \times G_s(\mathbf{r},\mathbf{r}_1;\omega_1+\omega)G_s(\mathbf{r}_1,\mathbf{r}';\omega_2+\omega) \times v(\mathbf{r}_1,\mathbf{r}_2)G_s(\mathbf{r}',\mathbf{r}_2;\omega_2)G_s(\mathbf{r}_2,r;\omega_1).$$

Carrying out the frequency integrals and converting to the retarded propagator in the upper half plane ($\omega\to z$ with $\mathrm{Im}\, z>0$) gives

$$R_V(\mathbf{r},\mathbf{r}';\omega) = -2\sum_{k_1k_2}\sum_{k_1'k_2'} \varphi_{k_1}(\mathbf{r})\varphi^*_{k_2}(\mathbf{r})\varphi^*_{k_1'}(\mathbf{r}')\varphi_{k_2'}(\mathbf{r}') \times \langle k_1k_2'|v|k_1'k_2\rangle \frac{(n_{k_1}-n_{k_2})(n_{k_1'}-n_{k_2'})}{(z+\varepsilon_{k_2}-\varepsilon_{k_1})(z+\varepsilon_{k_2'}-\varepsilon_{k_1'})}.$$

Here, the standard Coulomb integral is given by

$$\langle k_1k_2'|v|k_1'k_2\rangle = \int d^3r d^3r' \varphi^*_{k_1}(\mathbf{r})\varphi^*_{k_2'}(\mathbf{r}')v(\mathbf{r}-\mathbf{r}') \times \varphi_{k_1'}(\mathbf{r})\varphi_{k_2}(\mathbf{r}').$$

In the high-frequency limit, to leading order, this becomes B/ω^2 where the coefficient B is given by

$$B = -2\sum_{k_1k_2}\sum_{k_1'k_2'} \varphi_{k_1}(\mathbf{r})\varphi^*_{k_2}(\mathbf{r})\varphi^*_{k_1'}(\mathbf{r}')\varphi_{k_2'}(\mathbf{r}') \times \langle k_1k_2'|v|k_1'k_2\rangle (n_{k_1}-n_{k_2})(n_{k_1'}-n_{k_2'}).$$

Using again the completeness and the definition of the density matrix $n(\mathbf{r},\mathbf{r}')$ we obtain

$$B = -\delta(\mathbf{r}-\mathbf{r}')\int d^3\mathbf{r}_3 v(\mathbf{r}-\mathbf{r}_3)|n(\mathbf{r}_3,\mathbf{r})|^2 + v(\mathbf{r}-\mathbf{r}')|n(\mathbf{r},\mathbf{r}')|^2.$$

This is just the coefficient A, Eq. (A1), with the opposite sign. Consequently, the $1/z^2$ contribution from the vertex diagram exactly cancels the same term from the self-energy contributions meaning that $\chi_s f_x \chi_s$ decays as $1/z^4$ at large frequencies. And this provides an explicit proof of the f-sum rule in the EXX approximation.

Finally we note that this result means that the exchange kernel should have a very weak dependence on frequency at large frequencies.

[1] C. O. Almbladh, U. von Barth, and R. van Leeuwen, Int. J. Mod. Phys. B **13**, 535 (1999).
[2] U. von Barth, N. E. Dahlen, R. van Leeuwen, and G. Stefanucci, Phys. Rev. B **72**, 235109 (2005).
[3] S. Kurth and U. von Barth (unpublished).
[4] M. Hellgren and U. von Barth, Phys. Rev. B **76**, 075107 (2007).
[5] See, for instance, S. Albrecht, L. Reining, R. Del Sole, and G. Onida, Phys. Rev. Lett. **80**, 4510 (1998), and references therein.
[6] E. Runge and E. K. U. Gross, Phys. Rev. Lett. **52**, 997 (1984).
[7] M. Petersilka, U. J. Gossmann, and E. K. U. Gross, Phys. Rev. Lett. **76**, 1212 (1996).
[8] G. Onida, L. Reining, and A. Rubio, Rev. Mod. Phys. **74**, 601 (2002).
[9] N. T. Maitra, F. Zang, R. J. Cave, and K. Burke, J. Chem. Phys. **120**, 5932 (2004).
[10] L. Reining, V. Olevano, A. Rubio, and G. Onida, Phys. Rev. Lett. **88**, 066404 (2002).
[11] A. Marini, R. Del Sole, and A. Rubio, Phys. Rev. Lett. **91**, 256402 (2003).
[12] I. V. Tokatly and O. Pankratov, Phys. Rev. Lett. **86**, 2078 (2001).
[13] F. Bruneval, F. Sottile, V. Olevano, R. Del Sole, and L. Reining, Phys. Rev. Lett. **94**, 186402 (2005).
[14] Y.-H. Kim and A. Görling, Phys. Rev. Lett. **89**, 096402 (2002).
[15] Y. Shigeta, K. Hirao, and S. Hirata, Phys. Rev. A **73**, 010502(R) (2006).
[16] S. Hirata, S. Ivanov, I. Grabowski, and R. J. Bartlett, J. Chem. Phys. **116**, 6468 (2002).
[17] M. Petersilka, E. K. U. Gross, and K. Burke, Int. J. Quantum Chem. **80**, 534 (2000).
[18] T. Grabo, M. Petersilka, and E. K. U. Gross, J. Mol. Struct. **501**, 353 (2000).
[19] H. O. Wijewardane and C. A. Ullrich, Phys. Rev. Lett. **100**, 056404 (2008).
[20] A. Klein, Phys. Rev. **121**, 950 (1961).
[21] G. Baym, Phys. Rev. **127**, 1391 (1962).
[22] L. J. Sham and M. Schlüter, Phys. Rev. Lett. **51**, 1888 (1983).
[23] R. T. Sharp and G. K. Horton, Phys. Rev. **90**, 317 (1953).
[24] J. D. Talman and W. F. Shadwick, Phys. Rev. A **14**, 36 (1976).
[25] A. K. Rajagopal, Phys. Rev. A **6**, 1239 (1972).
[26] A. Holas, P. K. Aravind, and K. S. Singwi, Phys. Rev. B **20**, 4912 (1979).
[27] J. T. Devreese, F. Brosens, and L. F. Lemmens, Phys. Rev. B **21**,

1349 (1980).
[28] F. Brosens, J. T. Devreese, and L. F. Lemmens, Phys. Rev. B **21**, 1363 (1980).
[29] C. A. Ullrich, U. J. Gossmann, and E. K. U. Gross, Phys. Rev. Lett. **74**, 872 (1995).
[30] C. O. Almbladh and U. von Barth, Phys. Rev. B **31**, 3231 (1985).
[31] H. Jiang and E. Engel, J. Chem. Phys. **123**, 224102 (2005).
[32] Y. Niquet, M. Fuchs, and X. Gonze, Int. J. Quantum Chem. **101**, 635 (2004).
[33] S. Hirata, S. Ivanov, I. Grabowski, R. J. Bartlett, K. Burke, and J. D. Talman, J. Chem. Phys. **115**, 1635 (2001).
[34] S. Ivanov, S. Hirata, and R. J. Bartlett, J. Chem. Phys. **116**, 1269 (2002).
[35] E. Engel, H. Jiang, and A. F. Bonetti, Phys. Rev. A **72**, 052503 (2005).
[36] M. Stankovski, M.S. thesis, Lund University, 2002.
[37] H. Bachau, E. Cormier, P. Decleva, J. E. Hansen, and F. Martin, Rep. Prog. Phys. **64**, 1815 (2001).
[38] R. P. McEachran, A. G. Rymant, and A. D. Stauffer, J. Phys. B **10**, L681 (1977).
[39] E. Markiewicz, R. P. McEachran, and A. D. Stauffer, J. Phys. B **14**, 949 (1981).
[40] V. G. Kaveeshwar, K. T. Chung, and R. P. Hurst, Phys. Rev. **172**, 35 (1968).
[41] R. F. Stewart, J. Phys. B **8**, 1 (1975).
[42] A. Kumar and W. J. Meath, Mol. Phys. **54**, 823 (1985).
[43] S. G. Porsev and A. Derevianko, Phys. Rev. A **65**, 020701(R) (2002).
[44] R. F. Stewart, Mol. Phys. **30**, 745 (1975).
[45] S. J. Chakravorty, S. R. Gwaltney, E. R. Davidson, F. A. Parpia, and C. F. Fischer, Phys. Rev. A **47**, 3649 (1993).
[46] F. Aryasetiawan and O. Gunnarsson, Phys. Rev. B **66**, 165119 (2002).
[47] M. E. Casida, in *Recent Developments and Applications in Density Functional Theory*, edited by J. M. Seminario (Elsevier, Amsterdam, 1996).
[48] C. J. Umrigar and X. Gonze, Phys. Rev. A **50**, 3827 (1994).
[49] R. F. Stewart, Mol. Phys. **29**, 1577 (1975).
[50] M. Hindgren and C.-O. Almbladh, Phys. Rev. B **56**, 12832 (1997).
[51] L. Hedin, Phys. Rev. **139**, A796 (1965).